Article

Investigation of Mixed Convection in Spinning Nanofluid over Rotating Cone Using Artificial Neural Networks and BVP-4C Technique

Ali Hassan [1,*] **, Qusain Haider** [1,*] **, Najah Alsubaie** [2] **, Fahad M. Alharbi** [3] **, Abdullah Alhushaybari** [4] **and Ahmed M. Galal** [5,6]

1   Department of Mathematics, University of Gujrat, Gujrat 50700, Pakistan
2   Department of Computer Sciences, College of Computer and Information Sciences, Princess Nourah bint Abdulrahman University, P.O. Box 84428, Riyadh 11671, Saudi Arabia
3   Department of Mathematics, Al-Qunfudah University College, Umm Al-Qura University, Mecca, Saudi Arabia
4   Department of Mathematics, College of Science, Taif University, P.O. Box 11099, Taif 21944, Saudi Arabia
5   Department of Mechanical Engineering, College of Engineering in Wadi Alddawasir, Prince Sattam Bin Abdulaziz University, Saudi Arabia
6   Production Engineering and Mechanical Design Department, Faculty of Engineering, Mansoura University, Mansoura P.O. Box 35516, Egypt
*   Correspondence: muhammadali0544@gmail.com (A.H.); qusain.haider336@gmail.com (Q.H.)

Abstract: The significance of back-propagated intelligent neural networks (BINs) to investigate the transmission of heat in spinning nanofluid over a rotating system is analyzed in this study. The buoyancy effect is incorporated along with the constant thermophysical properties of nanofluids. Levenberg–Marquardt intelligent networks (ANNLMBs) are employed to study heat transmission by using a trained artificial neural network. The system of highly non-linear flow governing partial differential equations (PDEs) is transformed into ordinary differential equations (ODEs) which is taken as a system model. This achieved system model is utilized to generate data set using the "Adams" method for distinct scenarios of heat transmission investigation in a spinning nanofluid over a rotating system for the implementation of the proposed ANNLMB. Additionally, with the help of training, testing, and validation, the approximate solution of heat transmission in a spinning nanofluid in a rotating system is obtained using a BNN-based solver. The generated reference data achieved employing the proposed artificial neural network based on a Levenberg–Marquardt intelligent network is distributed in the following manner: training at 82%, testing at 9%, and validation at 9%. Furthermore, MSE, histograms, and regression analyses are performed to depict and discuss the impact of the varying influence of key parameters, such as unsteadiness "s" in spinning flow, Prandtl number effect "pr", the rotational ratio of nanofluid and cone α_1 and buoyancy effect γ_1 on velocities $F'G$ and temperature Θ profiles. The mean square error confirms the accuracy of the achieved results. Prandtl number and unsteadiness decrease the temperature profile and thermal boundary layer of the rotating nanofluid.

Keywords: neural networks; Levenberg–Marquardt neural network; heat transmission; spinning nanofluid; rotating system

MSC: 37M99

1. Introduction

Nanofluids have numerous applications in science and technology, such as wind turbine energy, engineering fields, dental applications, paper production industries, heat pipes, and solar collectors. Choi and Eastmann [1] coined the term "nanofluid" in 1995. In their study, they discovered that adding a nanometer-sized nano-particle, either metallic

or non-metallic, enhanced the thermal conductivity of the formed solution. Consequently, the heat transfer feature of the formed solution was enhanced. They named this newly formed solution "nanofluid." Rehman et al. [2] discussed the challenges and applications of nanofluids in various science and engineering fields. Wong and Leon [3] investigated the current and future applications of nanofluids. Xuan and Li [4] provided a concrete review of the heat transfer enhancement of nanofluids. Ganvir et al. [5] investigated the heat transfer properties of nanofluids.

Gowda et al. [6] explored Marangoni-driven boundary layer flow for heat and mass transfer with activation energy and chemical reactions. Varun Kumar et al. [7] analyzed the Arrhenius activation energy influence over the curved stretchable surface with hybrid nanofluids. Sarada et al. [8] investigated exponential heat generation with the Fourier heat flux model for water-based ternary hybrid nanofluids. Gowda et al. [9] illustrated the effect of the magnetic dipole on ferromagnetic fluid with a suction effect over a stretching surface. Umavathi et al. [10] explained the squeezing magneto-hydrodynamic flow of Casson fluid between convectively heated disks. Kumar et al. [11] investigated the Stefan blowing effect with a magnetic dipole on nanofluid over a stretchable surface. Kumar et al. [12] demonstrated three different nano-particle shape effects in a ternary hybrid nanofluid with heat transfer under a magnetic field effect. Some recent studies on nanofluids provide significant insight into heat transmission over distinct configurations [13–15].

The flow configuration involving the rotation of both fluid (nanofluid) and geometry (cone) has a plethora of applications in several fields. These applications include surgical implants [16], material engineering [17], nonlinear oscillators [18], and heat transfer enhancement [19,20]. Rekha et al. [21] demonstrated a hybrid nanofluid for cone, wedge, and plate under the activation energy effect. Hassan et al. [22] studied the thermal radiation effect on a hybrid nanofluid for PWT over a rotating cone. The natural convection of dusty nano-particles over a porous cone with non-linear temperature was discussed by Nabwey and Mahdy [23]. Gul et al. [24] examined hybrid nanofluid flow between the canonical gape between a cone and a rotating disk. Hussain et al. [25] elaborated on the magneto-hydrodynamic flow of carbon nanotubes over a rotating cone with a thermal radiation effect. Meena et al. [26] investigated mixed convection in the presence of a heat source and sink over a rotating cone. Mahdy et al. [27] illustrated natural convection over the porous cone with homogeneous and heterogeneous reactions. Heat and mass transfer in Jeffery fluid were explained by Saleem et al. [28] using a heat source and a chemical reaction over the cone. Here are some recent studies that involve rotating cone configurations for knowledge gains [29–32].

In recent years, different analytical and numerical methods, such as the homotopy analysis method, perturbation method, Rung–Kutta-4 method, finite difference schemes, BVP-4c technique, shooting method, spectral method, Keller box method, lattice Boltzmann method, finite volume method, and finite element method, have been extensively used to study different flow problems over different physiques. Apart from these numerical and analytical methods, scientists are now exploring the application of artificial neural networks to achieve more optimized and accurate results. Karimipour et al. [33] predicted the thermal conductivity of a hybrid nanofluid using an empirical data set and introduced a novel regression model of SVR. Shoaib et al. [34] discussed a back-propagated neural network to study ferro-fluid slip flow in the porous medium. Soomro et al. [35] studied magneto-hydrodynamic slip flow using an artificial neural network. Shoaib et al. [36], using intelligent neural networks, discussed entropy generation for Ree–Eyring fluid with ohmic heating effects. Raja et al. [37] examined mixed convection in a porous medium with entropy generation using intelligent neuro-computing.

He et al. [38] discussed the MHD effect on the slip velocity of nanofluid in a micro-channel using an artificial neural network and the lattice Boltzmann method. Safaei et al. [39] elaborated on the effect of temperature and concentration on the thermal conductivity of a hybrid nanofluid utilizing an artificial neural network. Khan et al. [40] described the nonlinear porous slip flow of nanofluids using artificial neural networks. Colak et al. [41]

modelled the bio-convective porous medium flow of Powell–Eyring nanofluid using an artificial neural network. Reddy et al. [42] investigated the entropy generation of MHD cross nanofluid using artificial neural networks. Toghraie et al. [43] predicted the viscosity of nanofluid using an artificial neural network at different temperatures and concentrations of nano-particles. Dey et al. [44] examined unsteady mixed convection over a circular cylinder in the presence of nanofluids using artificial neural networks.

The above literature review suggests that rotating flows have a plethora of applications in fields such as surgical implants [16], material engineering [17], nonlinear oscillators [18], and enhancement of heat transmission [19,20]. Hussain et al. [19] used the BVP-4c technique to discuss multi-based rotating nanofluids over a cone. Hassan et al. [20,22] analyzed the role of hybrid nano-particles in heat transfer enhancement over a rotating cone under magnetic and thermal radiation effects. The novelty of the present work is to examine heat transmission in different nanofluids over a spinning cone using artificial neural networks and the BVP-4c technique. Additionally, water is used as the base fluid for conveying silver (Ag) nano-particles. The flow governing equations were obtained using the stress tensor along with the boundary layer approximation. Additionally, the buoyancy effect is taken into account as a force that induces the rotating flow due to the temperature difference. Furthermore, Shoaib et al. [36] and Raja et al. [37] used ANN to investigate the impact of ohmic heating and mixed convection on entropy generation. Shoaib et al. [36] used the homotopy analysis method, whereas Raja et al. [37] employed the Adams method to generate reference data. Qureshi et al. [45] illustrated a complete description of Adams–Bashforth's method to generate the outcomes, whereas in this attempt, we have generated the reference data sets using the Adams method. Further, the novelty of this research is to design a soft computing artificial neural network based on a single Levenberg–Marquardt (ANNLMB) intelligent network for heat transmission in rotating Ag–water nanofluid in a spinning mechanism.

The following are key features of the present designed ANN procedures:

- The heat transmission in spinning nanofluids in a rotating system is investigated using back propagated neural networks (BNN) adopting trained ANN using Levenberg–Marquardt (LMB) through the mechanism of soft computing.
- The Adams' numerical method is utilized to generate the reference data set for the transmission of heat in spinning nanofluid over a rotating system by varying the unsteadiness of flow, buoyancy effect, rotational ratio, and Prandtl number for the designed BNNs-based ANNLMB scheme.
- To show the effectiveness, correctness, and characteristics of the designed artificial neural network, mean squared error, error histograms, and convergence curves are presented and discussed for the validity of the proposed scheme.

2. Mathematical Formulation of Rotating Flow

2.1. Problem Statement

Consider a rotating system in which a viscous, in-compressible flow is rotating about the axis of a spinning cone, as explained in Figure 1 above. The coordinates and configuration explained the direction and velocity components in their respective directions. The $u(t, x, z)$ component of velocity is in the tangential direction, the $v(t, x, z)$ component is considered along the circumference of the cone, and the $w(t, x, z)$ component of velocity is taken in the normal direction. Whereas α^* is the subtended angle of the cone, Ω_1, Ω_2 denote the fluid and cone's angular velocity, respectively.
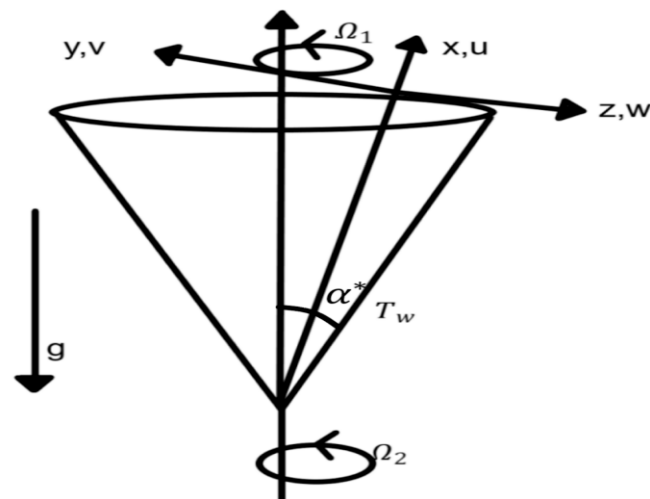
Figure 1. Physical configuration of rotating system.

2.2. Methodology to Obtain Flow Governing Equations

Flow governing general equations of unsteady viscous in-compressible nanofluid are given as follows [19,20,22]:

$$\nabla . V = 0, \tag{1}$$

$$\rho \frac{dV}{dt} = div\delta + f_b , \tag{2}$$

$$\rho C_p \frac{dT}{dt} = trace(\delta.L) - divq. \tag{3}$$

Here, V is the velocity vector, ∇ describes the divergence vector, ρ denotes density, $div\delta$ shows the stress tensor matrix, f_b depicts the body forces, C_p shows the heat capacity at constant pressure, $\frac{d}{dt} = \frac{\partial}{\partial t} + V.\nabla$ describes a material derivative of respective quantities, T defines temperature, and $divq$ denotes the heat flux, that is, $q = -\alpha \nabla T$. The Cauchy stress tensor used for the problem is as follows [19]:

$$\delta = -PI + \varepsilon , \quad \varepsilon = \mu A_1, \tag{4}$$

$$A_1 = \Pi + \Pi^t. \tag{5}$$

The boundary layer approximation theory along with the suitable viscous tensor are utilized to achieve the flow governing equations. This complete methodology is given by Hussain et al. [19]. Final flow governing equations are given as follows [19,20,22]:

$$x \frac{\partial u}{\partial x} + u + x \frac{\partial w}{\partial z} = 0, \tag{6}$$

$$\frac{\partial u}{\partial t} + u \frac{\partial u}{\partial x} + w \frac{\partial u}{\partial z} - \frac{v_e^2}{x} = -\frac{v_e^2}{x} + \nu_{nf} \left(\frac{\partial^2 u}{\partial z^2} \right) + g\xi cos\alpha^* (T - T_\infty), \tag{7}$$

$$\frac{\partial v}{\partial t} + u \frac{\partial v}{\partial x} + w \frac{\partial v}{\partial z} + \frac{vu}{x} = \frac{\partial v_e}{\partial t} + \nu_{nf} \left(\frac{\partial^2 v}{\partial z^2} \right), \tag{8}$$

$$\frac{\partial T}{\partial t} + u \frac{\partial T}{\partial x} + w \frac{\partial T}{\partial z} = \alpha_{nf} \left(\frac{\partial^2 T}{\partial z^2} \right). \tag{9}$$

Boundaries and initials conditions are given as [19,22]

$$
\begin{array}{cc}
\text{I.Cs} & \text{B.Cs} \\[4pt]
u(0,x,z) = u_i = -\dfrac{x(\Omega sin\alpha^*)f'(\eta)}{2} & u(t,x,0) = 0 \\[8pt]
v(0,x,z) = v_i = x(\Omega sin\alpha^*)g(\eta) & v(t,x,0) = \dfrac{\Omega sin\alpha^*}{(1-st\Omega sin\alpha^*)} \\[8pt]
w(0,x,z) = w_i = \dfrac{(\Omega sin\alpha^*)^{\frac{1}{2}}f(\eta)}{v^{\frac{1}{2}}} & w(t,x,0) = 0 \\[8pt]
T(0,x,z) = T_i = \dfrac{xcos\alpha^*\vartheta(\eta)}{L} & T(t,x,0) = T_w
\end{array}
\tag{10}
$$

Defining the following transformations [19,22]:

$$
\begin{gathered}
\eta = \frac{z\,(\Omega sin\alpha^*)^{0.5}}{v_f{}^{0.5}(1-st\Omega sin\alpha^*)^{0.5}},\ v_e = \frac{x\Omega_2 sin\alpha^*}{(1-st\Omega sin\alpha^*)},\ \alpha_1 = \frac{\Omega_1}{\Omega},\ t^* = t\Omega sin\alpha^*, \\[6pt]
Pr = \frac{v_f}{\alpha},\ u(t,x,z) = -\frac{x(\Omega sin\alpha^*)f'(\eta)}{2(1-st\Omega sin\alpha^*)},\ v = \frac{x(\Omega sin\alpha^*)g(\eta)}{(1-st\Omega sin\alpha^*)}, \\[6pt]
w = \frac{(\Omega sin\alpha^*)^{0.5}f(\eta)}{(1-st\Omega sin\alpha^*)^{0.5}v^{0.5}},\ \frac{T-T_\infty}{T_w-T_\infty} = \vartheta(\eta),\ \frac{T_w-T_\infty}{T_0-T_\infty} = \frac{x}{L}(1-st^*)^{-2}, \\[6pt]
T_w - T_\infty = \frac{x(T_0-T_\infty)cos\alpha^*}{L(1-st\Omega sin\alpha^*)^2},\ Re_L^2 = \Omega sin\alpha^* \frac{L^2}{v_f} \\[6pt]
G_{r_1} = g\xi cos\alpha^*(T_w - T_\infty)\frac{L^3}{v_f{}^2},\ \gamma_1 = \frac{Gr_1}{Re_L^2}.
\end{gathered}
\tag{11}
$$

Transformation methodology given in Equation (11) will transform Equations (7)–(9) in the following dimensionless form:

$$
F''' = (1-\varphi)^{2.5}\left(1-\varphi+\varphi*\left(\frac{\rho_s}{\rho_f}\right)\right)\left[s\left(F'-\frac{1}{2}\eta F''\right)-\frac{1}{2}F'^2+FF''+2(G^2-(1-\alpha_1)^2)+2\gamma_1\Theta\right],
\tag{12}
$$

$$
G'' = (1-\varphi)^{2.5}\left(1-\varphi+\varphi\left(\frac{\rho_s}{\rho_f}\right)\right)\left[s\left(G-\frac{1}{2}\eta G'\right)-GF'+FG'-s(1-\alpha_1)\right],
\tag{13}
$$

$$
\Theta'' = \left[(1-\varphi)+\varphi\left\{\frac{(\rho C_p)_s}{(\rho C_p)_f}\right\}\right]\left\{\frac{k_s+(n-1)k_f-\varphi(k_f-k_s)}{k_s+(n-1)k_f-(n-1)\varphi(k_f-k_s)}\right\}p_r\left[s\left(2\Theta+\frac{1}{2}\eta\Theta'\right)+F\Theta'-\frac{1}{2}F'\Theta\right].
\tag{14}
$$

Now the boundary conditions are:

$$
\begin{gathered}
F(0) = 0,\ F'(0) = 0,\ G(0) = \alpha_1,\ \Theta'(0) = -1, \\
F'(\infty) = 0,\ G(\infty) = 1-\alpha_1,\ \Theta'(\infty) = 0.
\end{gathered}
\tag{15}
$$

3. Methodology

In this section, the overview of proposed ANNLMB is presented to solve transformed flow governing Equations (12)–(14). The proposed ANNLMB is based on a single neural model concept to simulate the flow governing equations. The complete methodology is presented in two parts, the first part includes the generation of reference data set for the formulated problem of heat transmission in a spinning nanofluid over a rotating system. The reference datasets are generated with the help of Mathematica software using "NDSolver" and by employing the Adams method.

The numerically generated reference data set for velocity and temperature profiles is between 0 and 5, and the step size is taken as 0.05, i.e., 100 inputs for every varying parameter that include, Pr, α_1, γ_1 and s and given Table 1. In the second part, the proposed ANNLMB is demonstrated with the help of graphical user interface of neural network tool box using the "nftool" function in MATLAB. Training, testing and validation using the random values of inputs are set 82%, 9% and 9%, respectively.

Table 1. Scenarios for heat transmission in spinning nanofluid in rotating system.

Nanofluid Thermophysical Properties Utilized to Generate Reference Data, $\varphi = 0.01$ $\rho_s = 10490$, $\rho_f = 892$, $k_s = 429$, $k_f = 0.178$				
Numeric Values Used to Generate Reference Data				
Scenario	s	α_1	γ_1	pr
1	2	1	0.2	199
2	1	1	0.5	199
3	1	1	1	199
4	2	1	0.5	190

## 4. Interpretation of Results and Numerical Computation

Here, in this part, the outcomes achieved with the help of the proposed ANNLMB methodology for each scenario of heat transmission in a rotating nanofluid over a spinning mechanism are presented. Additionally, interpretations of obtained outcomes are also presented with graphical plots. Figure 2 depicts the structural configuration of the proposed ANNLMB, exploiting hidden layers of the neural network. The mathematical expression for the heat transmission of a spinning nanofluid in a rotating system for transformed flow governing Equations (12)–(15) can be written in simplified form for scenario 1 with help of numerical values presented in Table 1 below:

$$F''' = 1.03185593403 * \left[2 \times \left(F' - 0.5 \times F'' \right) - 0.5 \times F'^2 + FF'' + 2 \times \left(G^2 \right) + 2\gamma_1\Theta \right], \quad (16)$$

$$G'' = 1.03185593403 * \left[2 \times \left(G - 0.5 \times G' \right) - GF' + FG' - 2 \times (1 - \alpha_1) \right], \quad (17)$$

$$\Theta'' = \frac{199}{1.0407744214} \left[2 \times \left(2\Theta + 0.5 \times \eta\Theta' \right) + F\Theta' - 0.5 \times F'\Theta) \right]. \quad (18)$$
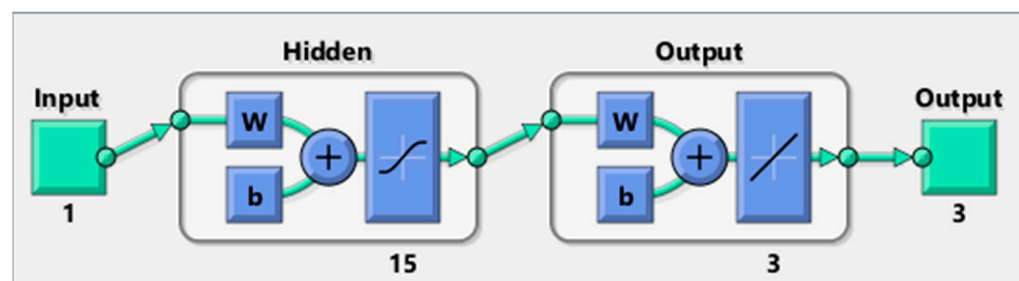
Figure 2. Networks structure of proposed ANNLMB Scheme.

The boundary conditions are given as

$$F(0) = 0, \ F'(0) = 0, \ G(0) = 1, \ \Theta'(0) = -1, \\ F'(\infty) = 0, \ G(\infty) = 0, \ \Theta'(\infty) = 0. \quad (19)$$

Similarly, mathematical expressions for all scenarios can be developed for heat transmission in a spinning nanofluid in a rotating system using data in Table 1 and Equations (12)–(14). Table 2 illustrates the comparison between the outcomes achieved for the present study and the previously published results by Hussain et al. [19], Raju and Sandeep [31]. The relations used in this study for the Nusselt number are similar to those used by [19]; therefore, we must omit them.

Table 2. Comparison of Nusselt number (Nu_x) with already published work of Hussain et al. [19]. Raju and Sandeep [31].

	Nu_x		
γ_1	Raju and Sandeep [31]	Hussain et al. [1]	Present
10	1.183409	1.37415	0.980211
15	1.337339	1.30846	1.202210
20	1.456372	1.34327	0.990011

Figure 3a–d represent MSE, mean square error, which is the average square value of difference between predicted results and reference standard outcome of Adams–Bashforth method, convergence performance or learning curves, i.e., update of MSE on step increment of epochs index of networks along with state-transition results of ANNLMB for all four scenarios, respectively. Figure 4a–d depict the state transition of the results. In these plots' gradient, step size Mu, and the maximum epochs performed are given for all four scenarios, respectively. Additionally, the comparison between the outcomes of ANNLMB and reference data for all four scenarios is presented in Figure 5a–d. The plots for histogram errors are depicted in Figure 6a–d. Furthermore, regression errors for all four scenarios are given in Figure 7a–d, respectively. The absolute error for all four scenarios is presented in Figure 8a–d. Tables 2–5 gives variation of convergence in terms of mean square error and time of execution.
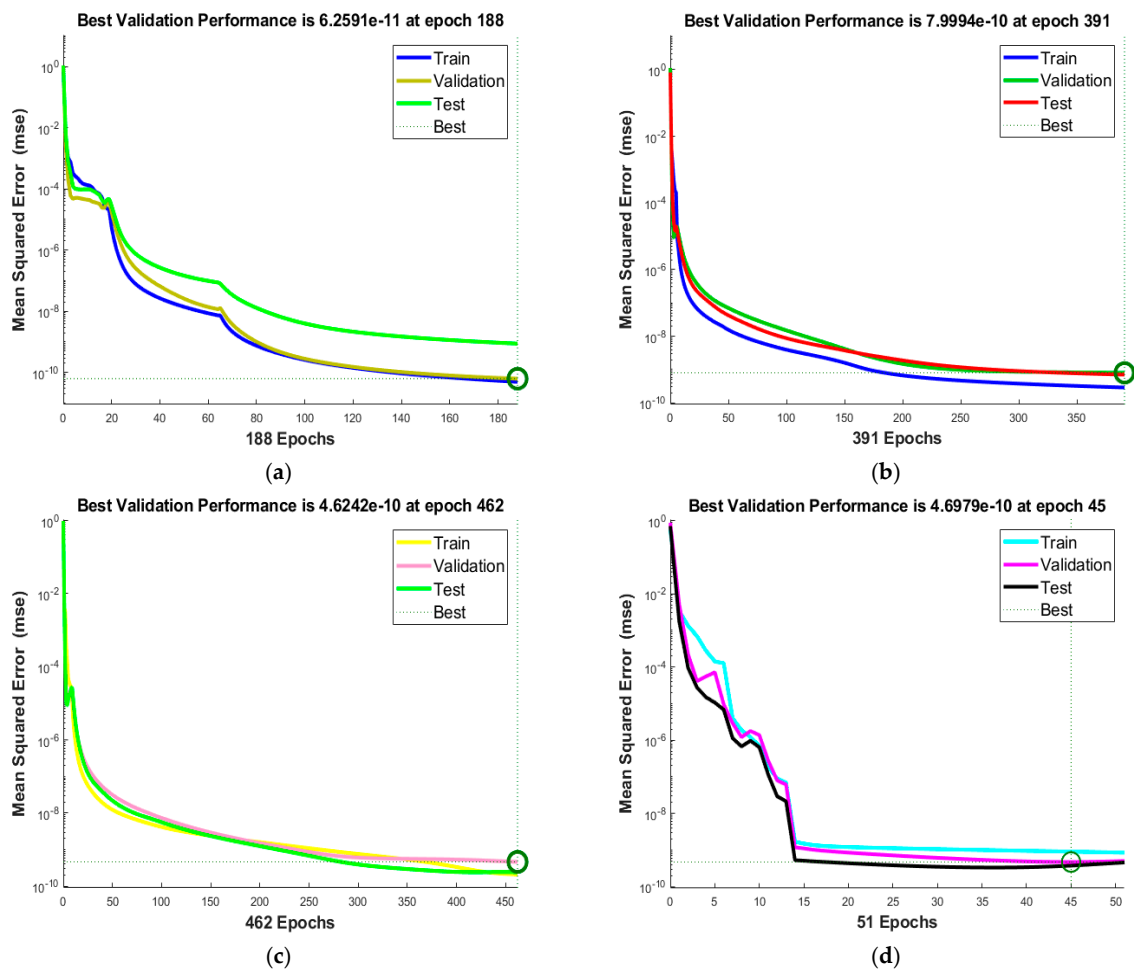
Figure 3. (**a**–**d**) Performance of MSE of proposed ANNLMB for solving heat transfer of spinning nanofluid. (**a**) MSE: Scenario 1; (**b**) MSE: Scenario 2; (**c**) MSE: Scenario 3; (**d**) MSE: Scenario 4.
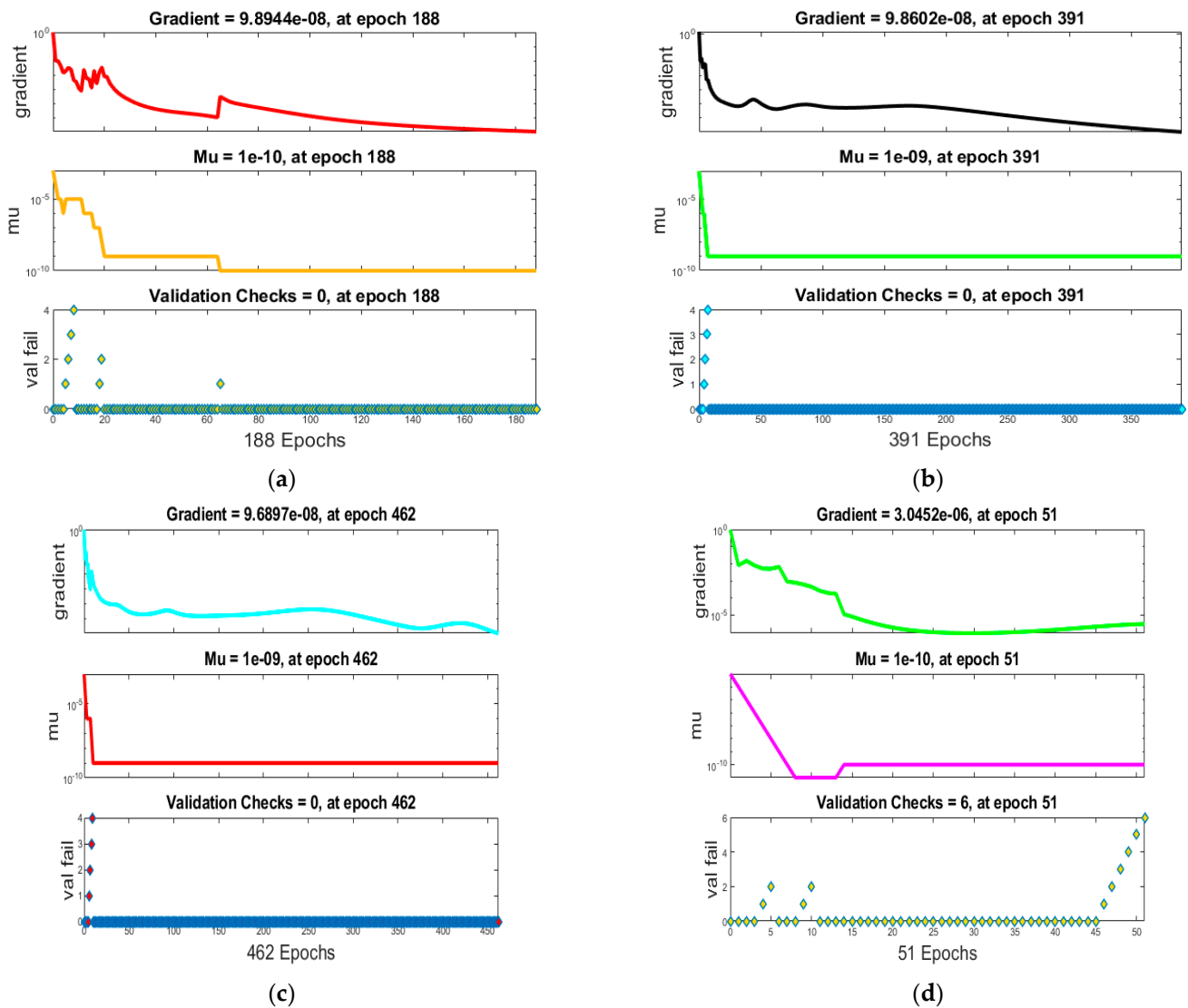
Figure 4. (**a**–**d**) Algorithm dynamics of ANNLMB to solving heat transfer of spinning nanofluid. (**a**) STR: Scenario 1; (**b**) STR: Scenario 2; (**c**) STR: Scenario 3; (**d**) STR: Scenario 4.
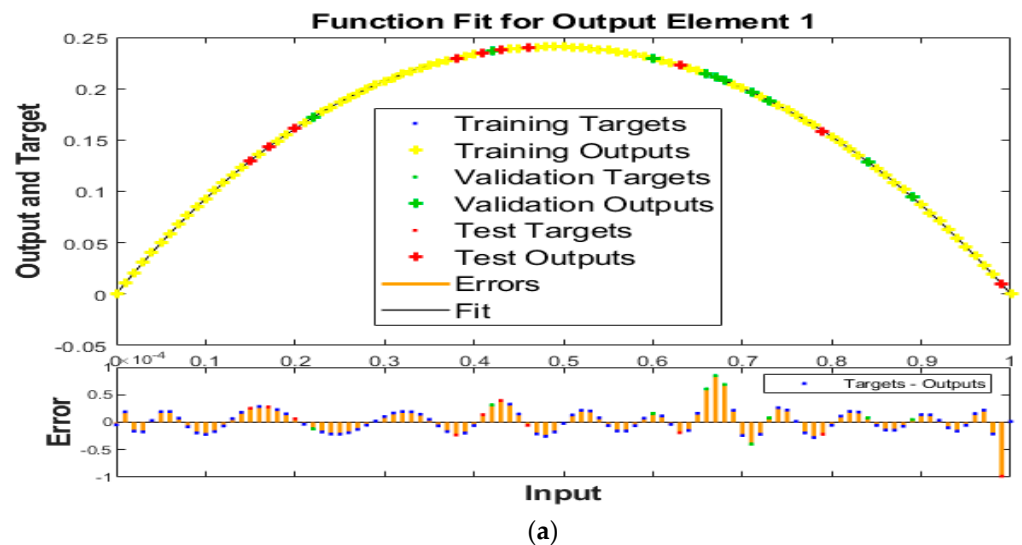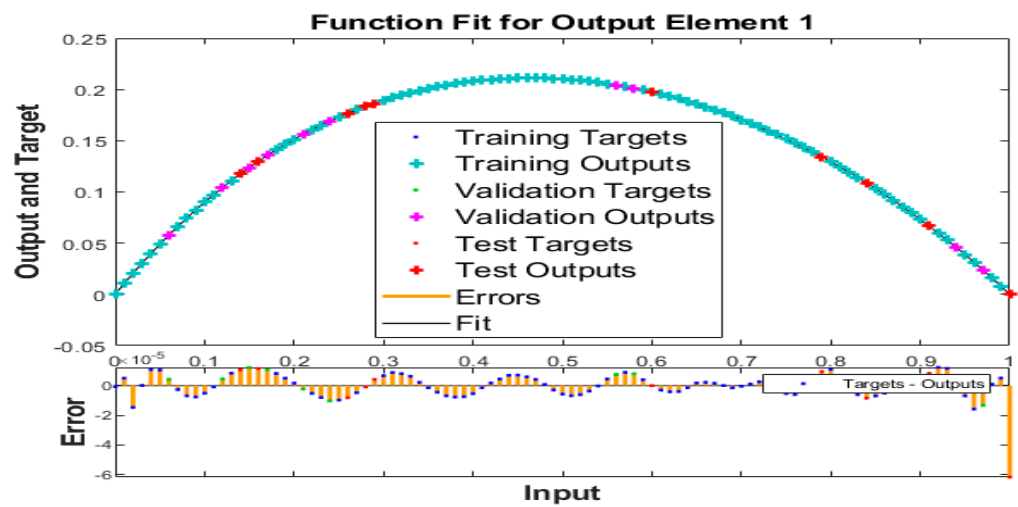

Figure 5. *Cont.*

(**b**)

(**c**)
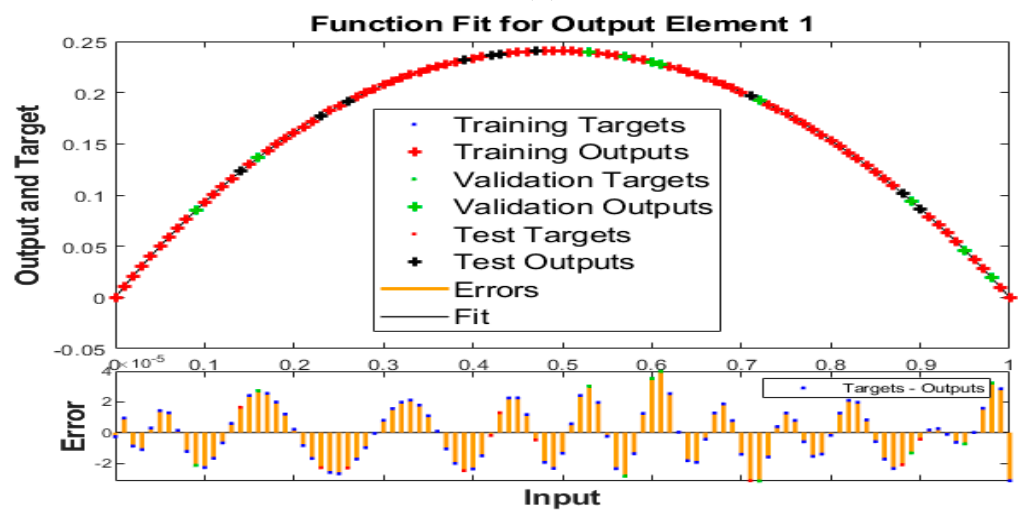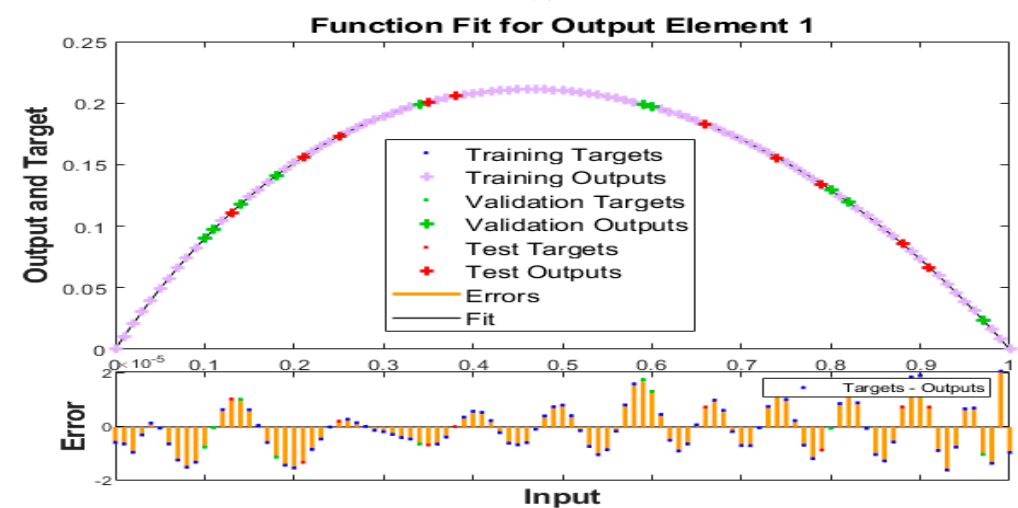

(**d**)

Figure 5. (**a**–**d**) ANNLMB outcome comparison from reference for different scenarios. (**a**) ANNLMB outcome comparison from reference for scenario 1; (**b**) ANNLMB outcome comparison from reference for scenario 1; (**c**) ANNLMB outcome comparison from reference for scenario 3; (**d**) ANNLMB outcome comparison from reference for scenario 4.
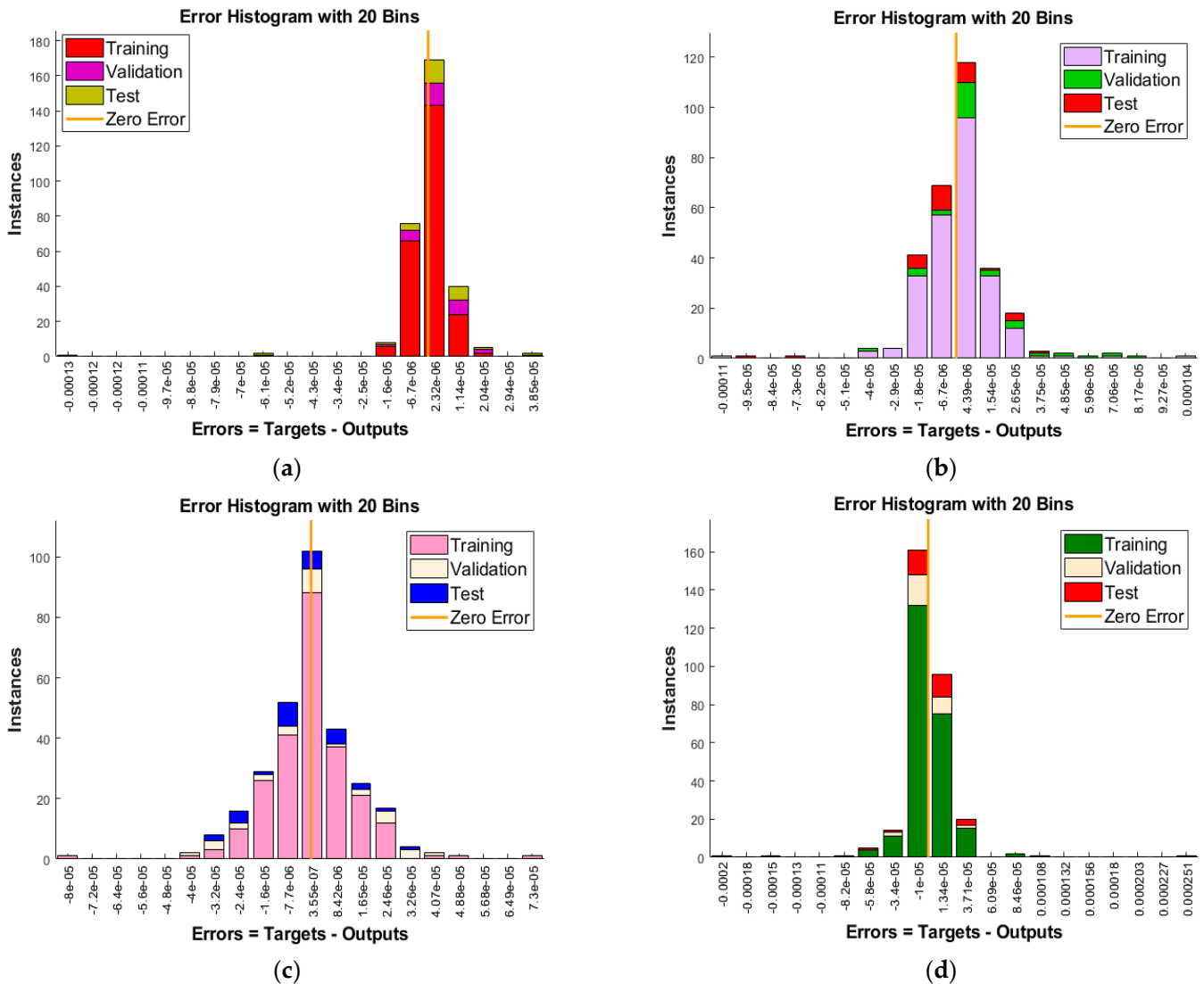
Figure 6. (**a**–**d**) Histograms for ANNLMB for each scenario of heat transfer in spinning nanofluid. (**a**) EH: Scenario 1; (**b**) EH: Scenario 2; (**c**) EH: Scenario 3; (**d**) EH: Scenario 4.

Table 3. ANNLMB outcomes of Scenario 1 for heat transfer in spinning nanofluid.

HLN	MSE Level			Performance Index	Value of Gradient	Step Size Mu	Executed Epochs	Time
	Training	Validation	Testing					
15	4.953×10^{-11}	6.259×10^{-11}	8.786×10^{-10}	4.95×10^{-11}	9.89×10^{-8}	1×10^{-10}	188	1 s

Table 4. ANNLMB outcomes of Scenario 2 for heat transfer in spinning nanofluid.

HLN	MSE Level			Performance Index	Value of Gradient	Step Size Mu	Executed Epochs	Time
	Training	Validation	Testing					
15	9.02241×10^{-10}	4.62417×10^{-10}	3.742×10^{-10}	2.90×10^{-10}	9.86×10^{-8}	1×10^{-9}	391	1 s
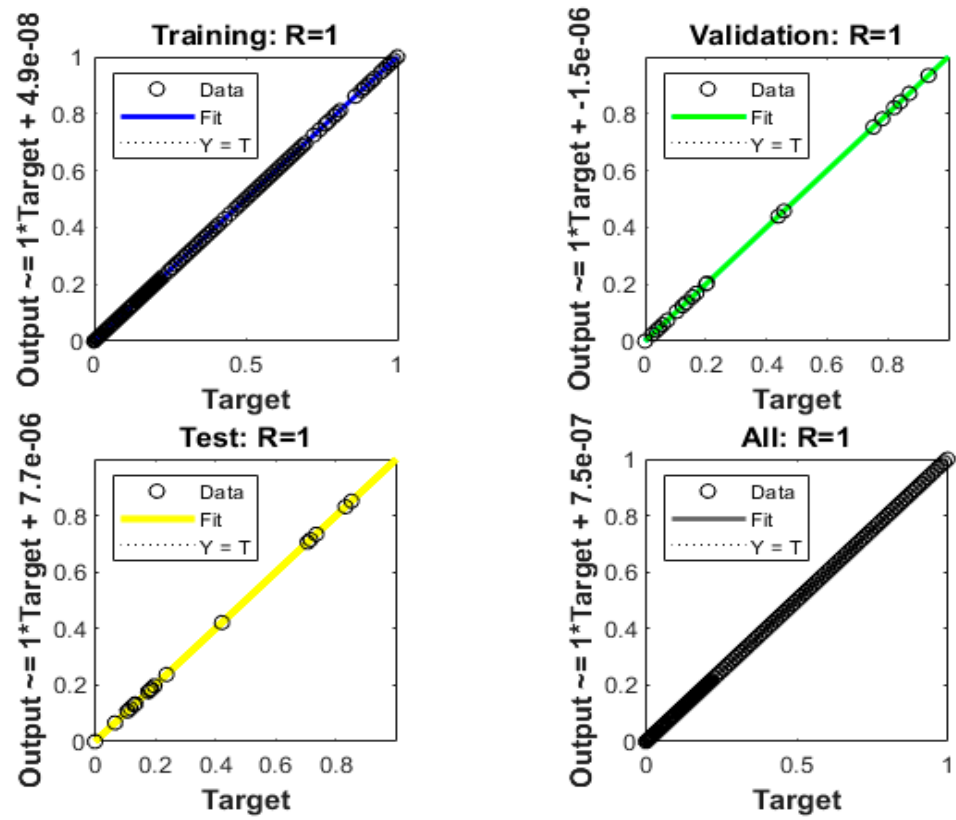
(**a**)

(**b**)

Figure 7. *Cont.*
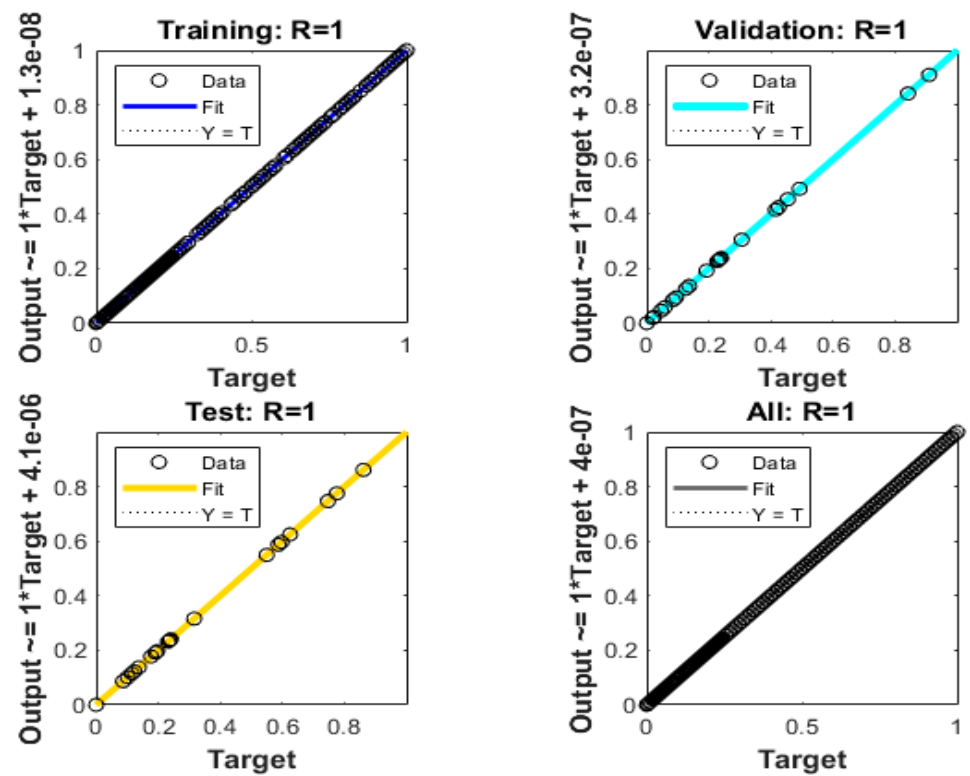
(**c**)
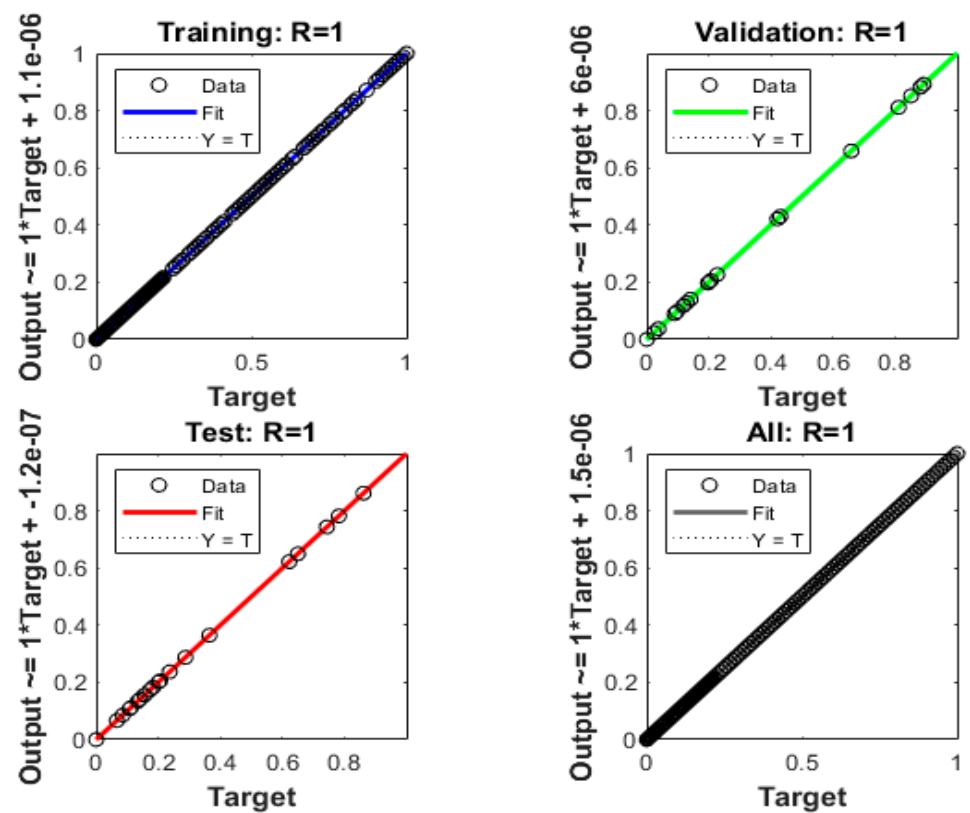
(**d**)

Figure 7. (**a**–**d**) ANNLMB outcome regression illustration of different scenarios. (**a**) ANNLMB outcome regression illustration of scenario 1; (**b**) ANNLMB outcome regression illustration of scenario 2; (**c**) ANNLMB outcome regression illustration of scenario 3; (**d**) ANNLMB outcome regression illustration of scenario 4.

Figure 8. (**a**–**d**) AE outcomes of ANNLMB for solving heat transfer in spinning nanofluid. (**a**) AE: Scenario 1; (**b**) AE: Scenario 2; (**c**) AE: Scenario 3; (**d**) AE: Scenario 4.

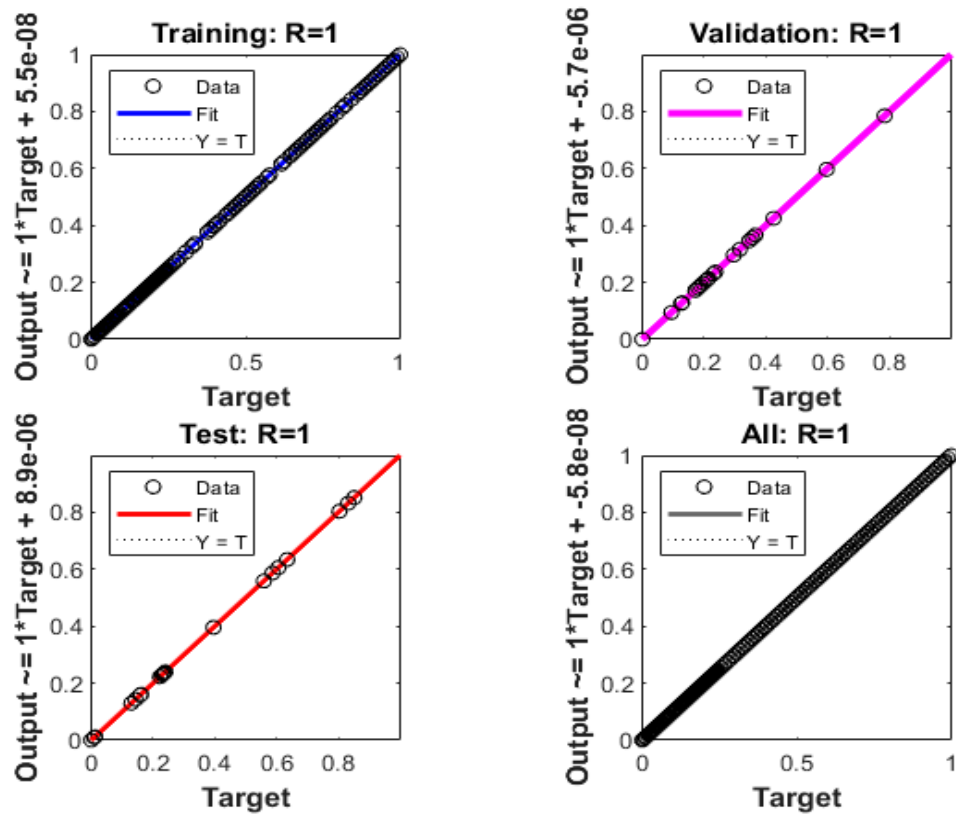**Table 5.** ANNLMB outcomes of Scenario 3 for heat transfer in spinning nanofluid.

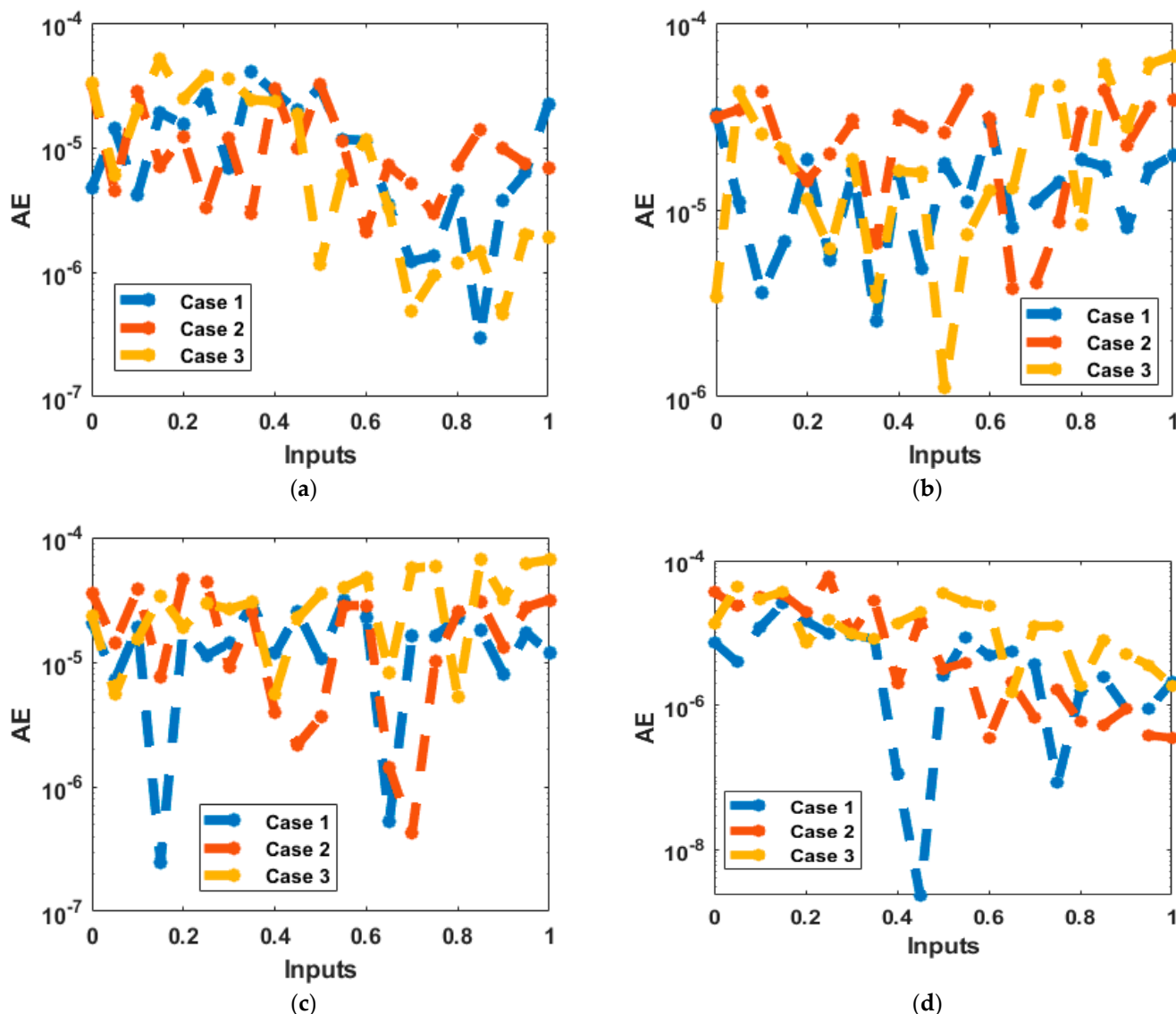| HLN	MSE Level			Performance Index	Value of Gradient	Step Size Mu	Executed Epochs	Time
	Training	Validation	Testing					
15	2.0914×10^{-10}	4.62417×10^{-10}	2.41862×10^{-10}	2.09×10^{-10}	9.69×10^{-8}	1×10^{-9}	462	1 s

The convergence analysis in terms of MSE for training, testing and validation is presented in Figure 3a–d for all four scenarios for the formulated heat transmission problem. It is observed from these plots that the convergence of the heat transmission problem is 10^{-10}, 10^{-9}, 10^{-9} and 10^{-9}, and it is achieved at 188, 391, 462, and 51 epochs for all four scenarios, respectively. Figure 4a–d demonstrate the gradient and step size *Mu* for all the four scenarios, respectively. The gradient obtained for all six scenarios are $\left[9.8944 \times 10^{-8}, 9.8602 \times 10^{-8}, 9.6897 \times 10^{-8}, \text{ and } 3.0452 \times 10^{-6} \right]$, whereas numerical values of *Mu* are $\left[10^{-10}, 10^{-9}, 10^{-9} \text{ and } 10^{-10} \right]$, respectively. These plots show the convergence as well as the accuracy of the ANNLMB for the formulated problem of heat transmission in a spinning nanofluid. Moreover, the stochastic nature of the ANNLMB algorithm is also observed by attaining invariable high-level accuracy in terms of the MSE

magnitude at different epoch numbers due to the randomness in the initialization of the back-propagation algorithm based on the Levenberg–Marquardt methodology. It is worth mentioning here that the outcomes obtained using proposed ANNLMB between 0 and 5 with a step size of 0.05 is compared with the reference solution using the "Adams" method. To illustrate the error between these two methods, comparison graphs are presented in Figure 5a–d for all four scenarios, respectively.

The maximum value of error obtained for training, testing and validation through the proposed ANNLMB is found to be 1×10^{-4}, 2×10^{-5}, 4×10^{-5} and 2×10^{-5} for all four of the scenarios of heat transmission in a spinning nanofluid in a rotating system, respectively. The error analysis was further discussed with the help of histograms for all four of the scenarios for training, testing and validation samples. Figure 6a–d illustrate histograms for all the four scenarios, respectively. The error bin with respect to the zero line contains error for all scenarios found to be with the range of 2.32×10^{-6}, 4.39×10^{-6}, 3.55×10^{-7}, and -1×10^{-5} for all three samples of training, testing and validation, which indicates the consistent and invariable accuracy of the proposed ANNLMB to solve heat transmission in a spinning nanofluid in a rotating system.

The co-relation studies are utilized to conduct the performance of regression. The outcomes of regression are given in Figure 7a–d for all four scenarios of heat transmission in a spinning nanofluid in a rotating system, respectively. The values of correlations of R are found to be in unity, which indicates the accurate value modeling for train, testing and validation. Moreover, this shows the perfect working environment of ANNLMB to compute and analyze heat transmission in a spinning nanofluid in a rotating system. Figure 8a–d depict the absolute error for the heat transmission in a nanofluid in a rotating system. It is concluded from the plots (a–d) that errors are found to be in the range of 10^{-4} to 10^{-7}, 10^{-4} to 10^{-6}, 10^{-4} to 10^{-7}, and 10^{-4} to 10^{-8}, respectively. These generated absolute error for all four scenarios confirms the validity of the obtained results for heat transmission in a spinning nanofluid in a rotating system. The performance of ANNLMB can be seen in Tables 2–5. The performance of scenario 1 is up to 10^{-11}, for scenario 2, 10^{-10}, for scenario 3, it is up to 10^{-10}, and for scenario 4, it is 10^{-10} for heat transmission in a spinning nanofluid in a rotating system. These outcomes illustrate that the performance of ANNLMB is consistent throughout the varying scenarios for problem under observation.

Velocity and Temperature Profiles

Figure 9a,b describe the effect of the rotation ratio and unsteadiness on motion profiles of a spinning nanofluid in a rotating system, respectively. Figure 9a depicts the impact of the rotational ratio on the primary velocity profile. It is observed that when the rotation of flow in the rotating flow mechanism is enhanced, the primary velocity profile decreases. Additionally, the associated momentum boundary layer thickness also starts to decrease with the increment in the rotational ratio of the fluid and cone. Figure 9b shows the effect of the rotational ratio on the secondary velocity profile. The secondary velocity profile is decreased with the increment in the flow rotational ratio. It is also worth noting here that with increment in the rotational ratio, contraction in the thickness of the associated momentum boundary layer is observed. Figure 9c,d demonstrate the effect of unsteadiness in the motion profiles of a spinning nanofluid in a rotating system. Figure 9c describes the effect of the unsteadiness parameter on the primary velocity. It is worth noting that as the unsteadiness in the spinning nanofluid motion is enhanced, the thickness of the momentum boundary expands dramatically. The motion of Ag/water nanofluid is abruptly decreased. Furthermore, Figure 9d shows the impression of the unsteadiness influence on the secondary velocity profile. The secondary velocity is increased abruptly with the increment in unsteadiness in the motion of the spinning nanofluid flow.

Figure 9e illustrates the effect of the Prandtl number and unsteadiness on the temperature profile, respectively. It is observed that with the increment in the Prandtl number, the temperature profile starts to gradually decrease. Additionally, the associated thermal boundary layer thickness is decreased with the increment in the Prandtl number. Figure 9f

reports the influence of unsteadiness on the temperature profile of the rotating nanofluid. It is worth noting here that with the increment in unsteadiness, the temperature profile is decreased. The thermal boundary of rotating nanofluid is decreased with the increment in the unsteadiness parameter. Table 6 below illustrate heat transfer outcomes using ANN-LMB for spinning nanofluids.

Table 6. ANNLMB outcomes of scenario 4 for heat transfer in spinning nanofluid.

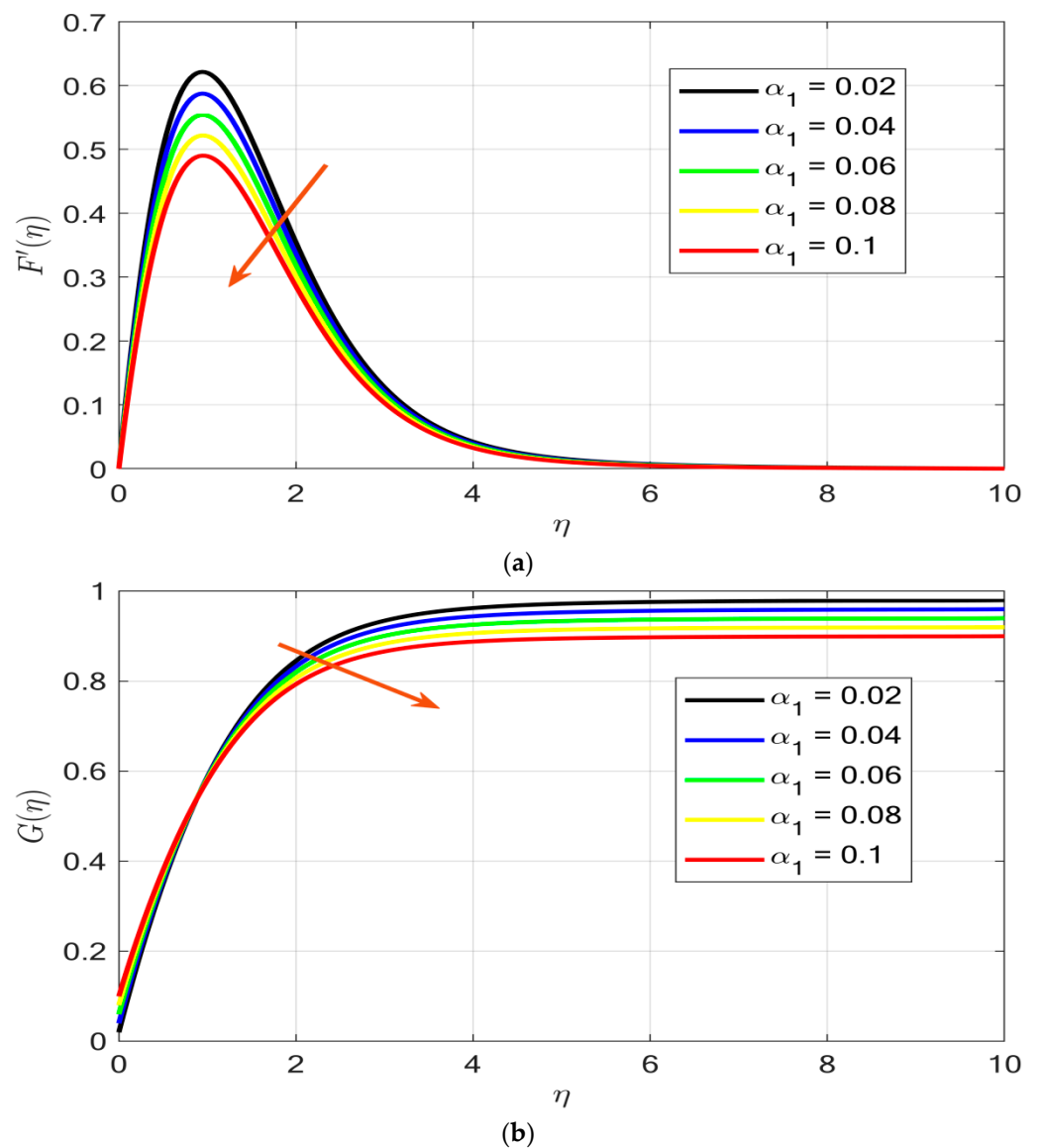| HLN	MSE Level			Performance Index	Value of Gradient	Step Size Mu	Executed Epochs	Time
	Training	Validation	Testing					
15	2.90472×10^{-10}	7.99939×10^{-10}	7.07677×10^{-10}	8.47×10^{-10}	3.05×10^{-6}	1×10^{-10}	51	1 s

(a)

(b)

Figure 9. *Cont.*

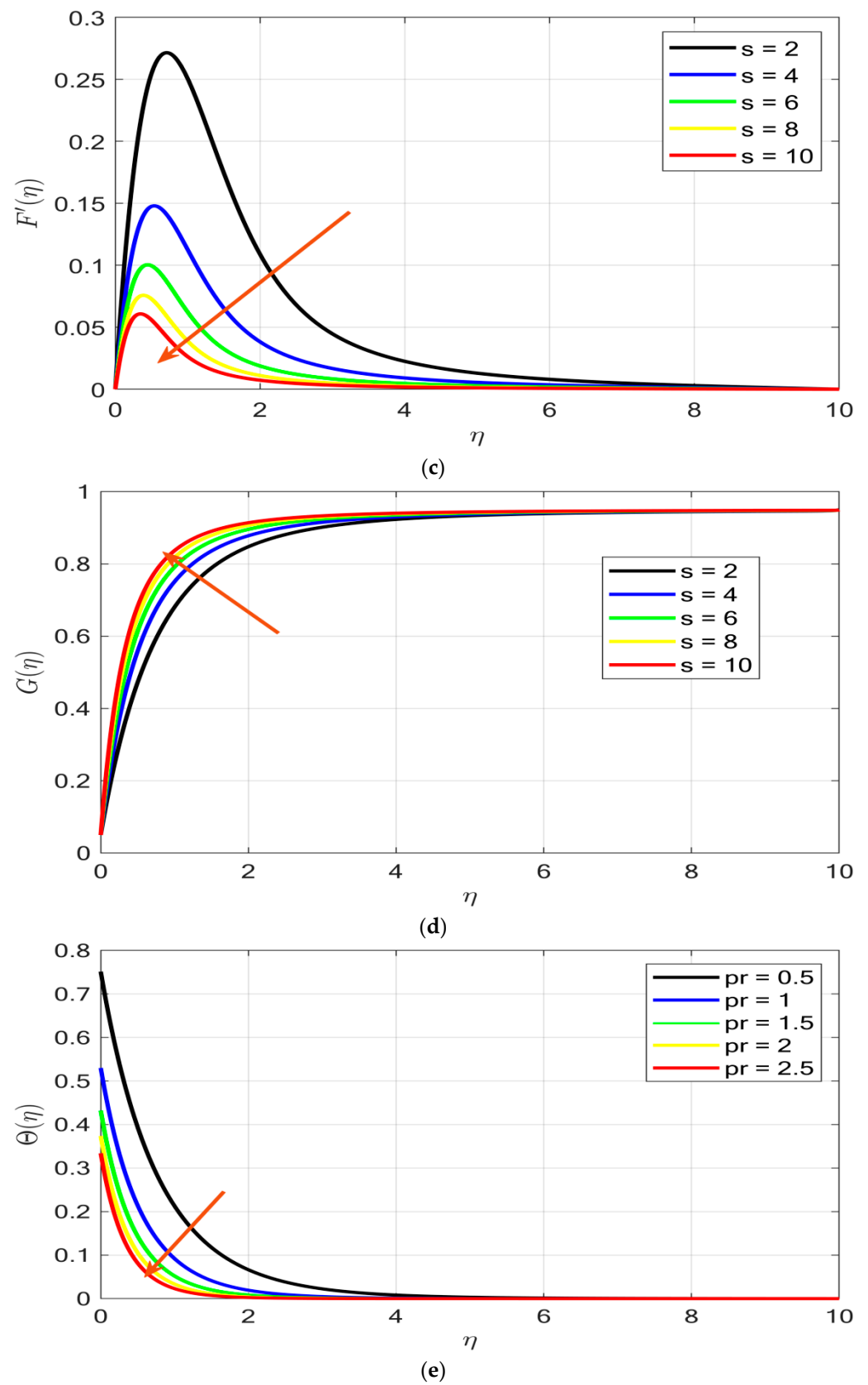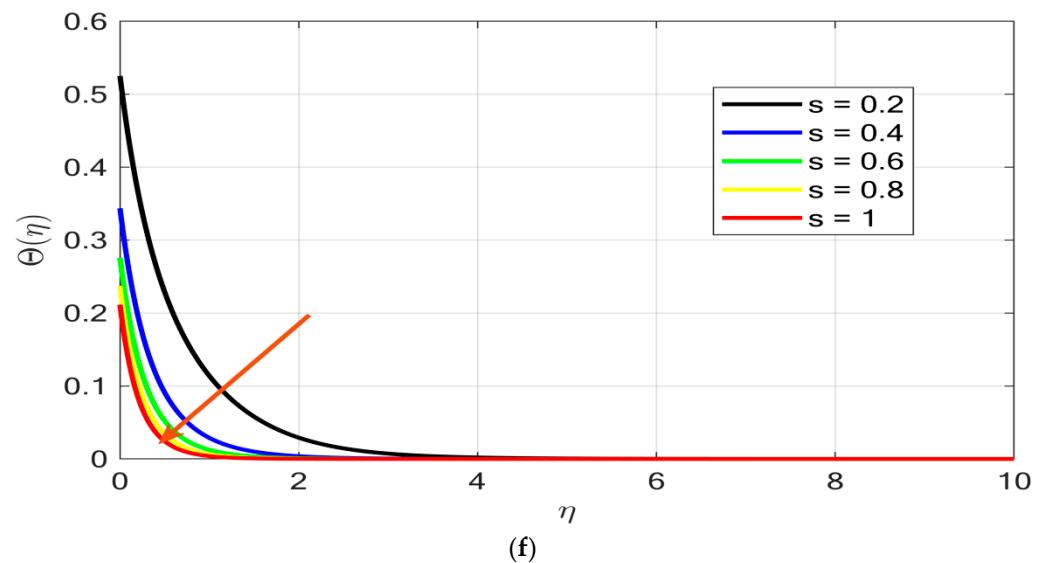(**c**)

(**d**)

(**e**)

Figure 9. *Cont.*

(f)

Figure 9. (**a**–**f**) Demonstration of distinct varying parameters on study profiles. (**a**) Influence of rotational ratio on primary velocity; (**b**) impact of rotational ratio on primary velocity; (**c**) impression of rotational ratio on primary velocity; (**d**) depiction of rotational ratio on primary velocity; (**e**) influence of Prandtl number on temperature profile; (**f**) effect of unsteadiness on temperature profile.

5. Conclusions

In this study, heat transmission in a rotating Ag/water nanofluid in a spinning cone system was investigated with the help of intelligent soft computing based on Levenberg–Marquardt networks. Through the proposed ANN-LMB artificial neural networks, it is observed that ANNs based on LMB provide more effective and accurate results. Additionally, the Adams method is utilized in this study to generate the reference data for heat transmission in nanofluid over a rotating cone system. The proposed ANNLMB is highly accurate and also provides significant insight into the MSE, along with a comparison between the outcomes of the Adams method and the results achieved through the proposed ANNLMB methodology. Convergence analysis, illustration of mean square error outcomes, and performance comparison are some of the key outcomes of the proposed ANNLMB methodology. There are very few implications of the proposed ANNLMB, such as the unavailability of larger reference data sets and errors in the generated data sets. The following are the major outcomes of the study:

- The outcomes of proposed ANNLMB are in complete agreement with reference data at 10^{-10} to 10^{-11}. This fact verifies and validates the effectiveness and correctness of the proposed ANNLMB to investigate the heat transmission in a spinning nanofluid in a rotating system.
- Verification of proposed ANNLMB scheme is further validated by providing numerical and graphical illustrations in terms of MSE, AH and index of regression.
- It is observed that with the increment in the rotational ratio, the primary velocity decreases, whereas an inclination is attained for the secondary velocity profile. The presence of high unsteadiness force in fluid motion dramatically declines the primary motion profile, while a sharp increase is observed in the secondary motion profile.
- The momentum boundary layer expands with an increment in the rotational ratio and unsteadiness in motion in the primary velocity profile. Additionally, contraction is attained for secondary velocity profile.
- Augmentation in the Prandtl number and unsteadiness parameter decrease the temperature profile sharply. Further, the thermal boundary layer thickness decreases with the increment in the Prandtl number and unsteadiness parameter.

Future Interest

The authors hope to use artificial neural networks (ANNs) in the future to investigate fractional and integer-order fluid mechanics problems. Additionally, infectious disease models could be an interesting area to explore using ANNs.

Author Contributions: Conceptualization, A.H. and Q.H.; methodology, A.H. and Q.H.; software, A.H. and Q.H.; validation, A.H., F.M.A. and A.A.; formal analysis, A.A., N.A. and A.M.G.; investigation, A.H.; resources, N.A., A.A., A.M.G. and F.M.A.; data curation, A.H. and Q.H.; writing—original draft preparation, A.H.; visualization, and A.M.G.; supervision, A.H.; writing review and editing, A.H.; project administration, A.H.; funding acquisition, N.A., A.A., A.M.G. and F.M.A. All authors have read and agreed to the published version of the manuscript.

Data Availability Statement: The data will be made available upon request.

Conflicts of Interest: The authors declare that there is no conflict of interest.

Nomenclature

u, v, w	Velocities components in respective direction (ms^{-1})	$(\rho c_p)_f$	Volumetric heat capacity of base fluid (JK^{-1})
v_f	Kinematic viscosity of base fluid $(m^2 s^{-1})$	$(\rho C_p)_{nf}$	Volumetric heat capacity of nanofluids (JK^{-1})
ρ_f	The density of base fluids (kgm^{-3})	T_W, T_∞	Wall and Ambient temperature (K)
C_p	Heat capacity at constant pressure $(Jkg^{-1}K^{-1})$	α^*	Angle of cone $(degree)$
ρ_{nf}	Density of nanoparticles (kgm^{-3})	μ_f	Dynamic viscosity $(kgm^{-1}s^{-1})$
∇	Gradient vector	V	Velocity in vector form (ms^{-1})
F, G	Primary and secondary velocity $[-]$	Θ	Temperature profile $[-]$
Ω	Composite angular velocity $[-]$	pr	Prandtl Number $[-]$
Ω_1, Ω_2	Rotational velocity of cone and fluid, respectively $[-]$	γ_1	Buoyancy parameter $[-]$
α_1	Rotation parameter $[-]$	Re_L	Reynolds number $[-]$
η	Similarity variable $[-]$	ODE's	Ordinary differential equations
MSE	Mean square error	BLA	Boundary layer approximation
PDE's	Partial differential equations		

References

1. Choi, S.U.; Eastman, J.A. *Enhancing Thermal Conductivity of Fluids with Nanoparticles*; Argonne National Lab. (ANL): Argonne, IL, USA, 1995.
2. Saidur, R.; Leong, K.; Mohammed, H. A review on applications and challenges of nanofluids. *Renew. Sustain. Energy Rev.* **2011**, *15*, 1646–1668. [CrossRef]
3. Wong, K.V.; De Leon, O. Applications of nanofluids: Current and future. *Adv. Mech. Eng.* **2010**, *2*, 519659. [CrossRef]
4. Xuan, Y.; Li, Q. Heat transfer enhancement of nanofluids. *Int. J. Heat Fluid Flow* **2000**, *21*, 58–64. [CrossRef]
5. Ganvir, R.; Walke, P.; Kriplani, V. Heat transfer characteristics in nanofluid—A review. *Renew. Sustain. Energy Rev.* **2017**, *75*, 451–460. [CrossRef]
6. Punith Gowda, R.J.; Naveen Kumar, R.; Jyothi, A.M.; Prasannakumara, B.C.; Sarris, I.E. Impact of binary chemical reaction and activation energy on heat and mass transfer of marangoni driven boundary layer flow of a non-Newtonian nanofluid. *Processes* **2021**, *9*, 702. [CrossRef]
7. Kumar, R.V.; Alhadhrami, A.; Gowda, R.P.; Prasannakumara, B. Exploration of Arrhenius activation energy on hybrid nanofluid flow over a curved stretchable surface. *ZAMM-J. Appl. Math. Mech.* **2021**, *101*, e202100035.
8. Sarada, K.; Gamaoun, F.; Abdulrahman, A.; Paramesh, S.O.; Kumar, R.; Prasanna, G.D.; Gowda, R.P. Impact of exponential form of internal heat generation on water-based ternary hybrid nanofluid flow by capitalizing non-Fourier heat flux model. *Case Stud. Therm. Eng.* **2022**, *38*, 102332.
9. Gowda, R.P.; Kumar, R.N.; Prasannakumara, B.C.; Nagaraja, B.; Gireesha, B.J. Exploring magnetic dipole contribution on ferromagnetic nanofluid flow over a stretching sheet: An application of Stefan blowing. *J. Mol. Liq.* **2021**, *335*, 116215. [CrossRef]
10. Umavathi, J.C.; Prakasha, D.G.; Alanazi, Y.M.; Lashin, M.M.; Al-Mubaddel, F.S.; Kumar, R.; Punith Gowda, R.J. Magnetohydrodynamic squeezing Casson nanofluid flow between parallel convectively heated disks. *Int. J. Mod. Phys. B* **2022**, 2350031. [CrossRef]

11. Kumar, R.N.; Gowda, R.P.; Prasannakumara, B.C.; Raju, C.S.K. Stefan Blowing Effect on Nanofluid Flow over a Stretching Sheet in the Presence of a Magnetic Dipole. In *Micro and Nanofluid Convection with Magnetic Field Effects for Heat and Mass Transfer Applications Using Matlab*; Elsevier: Amsterdam, The Netherlands, 2022; pp. 91–111.

12. Kumar, R.N.; Gamaoun, F.; Abdulrahman, A.; Chohan, J.S.; Gowda, R.J.P. Heat transfer analysis in three-dimensional unsteady magnetic fluid flow of water-based ternary hybrid nanofluid conveying three various shaped nanoparticles: A comparative study. *Int. J. Mod. Phys. B* **2022**, *36*, 2250170. [CrossRef]

13. Arshad, M.; Hussain, A.; Hassan, A.; Khan, I.; Badran, M.; Mehrez, S.; Elfasakhany, A.; Abdeljawad, T.; Galal, A.M. Heat Transfer Analysis of Nanostructured Material Flow over an Exponentially Stretching Surface: A Comparative Study. *Nanomaterials* **2022**, *12*, 1204. [CrossRef] [PubMed]

14. Arshad, M.; Hussain, A.; Hassan, A.; Shah, S.A.G.A.; Elkotab, M.A.; Gouadria, S.; Alsehli, M.; Galal, A.M. Heat and mass transfer analysis above an unsteady infinite porous surface with chemical reaction. *Case Stud. Therm. Eng.* **2022**, *36*, 102140. [CrossRef]

15. Arshad, M.; Hussain, A.; Shah, S.A.G.A.; Wróblewski, P.; Elkotb, M.A.; Abdelmohimen, M.A.; Hassan, A. Thermal energy investigation of magneto-hydrodynamic nano-material liquid flow over a stretching sheet: Comparison of single and composite particles. *Alex. Eng. J.* **2022**, *61*, 10453–10462. [CrossRef]

16. Raju, C.S.K.; Sandeep, N.; Sugunamma, V. Unsteady magneto-nanofluid flow caused by a rotating cone with temperature dependent viscosity: A surgical implant application. *J. Mol. Liq.* **2016**, *222*, 1183–1191. [CrossRef]

17. Hanif, H.; Khan, I.; Shafie, S. A novel study on time-dependent viscosity model of magneto-hybrid nanofluid flow over a permeable cone: Applications in material engineering. *Eur. Phys. J. Plus* **2020**, *135*, 730. [CrossRef]

18. Nawaz, Y.; Arif, M.S. Generalized decomposition method: Applications to nonlinear oscillator and MHD fluid flow past cone/wedge geometries. *Numer. Heat Transf. Part B Fundam.* **2020**, *77*, 42–63. [CrossRef]

19. Hussain, A.; Hassan, A.; Arshad, M.; Rehman, A.; Matoog, R.T.; Abdeljawad, T. Numerical simulation and thermal enhancement of multi-based nanofluid over an embrittled cone. *Case Stud. Therm. Eng.* **2021**, *28*, 101614. [CrossRef]

20. Hassan, A.; Hussain, A.; Arshad, M.; Haider, Q.; Althobaiti, A.; Elagan, S.K.; Alqurashi, M.S.; Abdelmohimen, M.A. Heat transport investigation of hybrid nanofluid (Ag-CuO) porous medium flow: Under magnetic field and Rosseland radiation. *Ain Shams Eng. J.* **2022**, *13*, 101667. [CrossRef]

21. Rekha, M.B.; Sarris, I.E.; Madhukesh, J.K.; Raghunatha, K.R.; Prasannakumara, B.C. Activation energy impact on flow of AA7072-AA7075/Water-Based hybrid nanofluid through a cone, wedge and plate. *Micromachines* **2022**, *13*, 302. [CrossRef]

22. Hassan, A.; Hussain, A.; Arshad, M.; Alanazi, M.M.; Zahran, H.Y. Numerical and Thermal Investigation of Magneto-Hydrodynamic Hybrid Nanoparticles (SWCNT-Ag) under Rosseland Radiation: A Prescribed Wall Temperature Case. *Nanomaterials* **2022**, *12*, 891. [CrossRef]

23. Nabwey, H.A.; Mahdy, A. Numerical approach of micropolar dust-particles natural convection fluid flow due to a permeable cone with nonlinear temperature. *Alex. Eng. J.* **2021**, *60*, 1739–1749. [CrossRef]

24. Gul, T.; Bilal, M.; Alghamdi, W.; Asjad, M.I.; Abdeljawad, T. Hybrid nanofluid flow within the conical gap between the cone and the surface of a rotating disk. *Sci. Rep.* **2021**, *11*, 1180. [CrossRef] [PubMed]

25. Hussain, A.; Hassan, A.; Al Mdallal, Q.; Ahmad, H.; Rehman, A.; Altanji, M.; Arshad, M. Heat transport investigation of magneto-hydrodynamics (SWCNT-MWCNT) hybrid nanofluid under the thermal radiation regime. *Case Stud. Therm. Eng.* **2021**, *27*, 101244. [CrossRef]

26. Meena, O.P.; Janapatla, P.; Srinivasacharya, D. Mixed Convection Flow across a Vertical Cone with Heat Source/Sink and Chemical Reaction Effects. *Math. Model. Comput. Simul.* **2022**, *14*, 532–546. [CrossRef]

27. Mahdy, A. Aspects of homogeneous-heterogeneous reactions on natural convection flow of micropolar fluid past a permeable cone. *Appl. Math. Comput.* **2019**, *352*, 59–67. [CrossRef]

28. Saleem, S.; Al-Qarni, M.M.; Nadeem, S.; Sandeep, N. Convective heat and mass transfer in magneto Jeffrey fluid flow on a rotating cone with heat source and chemical reaction. *Commun. Theor. Phys.* **2018**, *70*, 534. [CrossRef]

29. Reddy, P.S.; Chamkha, A. Heat and mass transfer analysis in natural convection flow of nanofluid over a vertical cone with chemical reaction. *Int. J. Numer. Methods Heat Fluid Flow* **2017**, *27*, 2–22. [CrossRef]

30. Anilkumar, D.; Roy, S. Unsteady mixed convection flow on a rotating cone in a rotating fluid. *Appl. Math. Comput.* **2004**, *155*, 545–561. [CrossRef]

31. Raju, C.S.K.; Sandeep, N. Opposing and assisting flow characteristics of radiative Casson fluid due to cone in the presence of induced magnetic field. *Int. J. Adv. Sci. Technol.* **2016**, *88*, 43–62. [CrossRef]

32. Nadeem, S.; Saleem, S. Mixed convection flow of Eyring–Powell fluid along a rotating cone. *Results Phys.* **2014**, *4*, 54–62. [CrossRef]

33. Karimipour, A.; Bagherzadeh, S.A.; Taghipour, A.; Abdollahi, A.; Safaei, M.R. A novel nonlinear regression model of SVR as a substitute for ANN to predict conductivity of MWCNT-CuO/water hybrid nanofluid based on empirical data. *Phys. A Stat. Mech. Its Appl.* **2019**, *521*, 89–97. [CrossRef]

34. Shoaib, M.; Kausar, M.; Khan, M.I.; Zeb, M.; Gowda, R.P.; Prasannakumara, B.; Alzahrani, F.; Raja, M.A.Z. Intelligent backpropagated neural networks application on Darcy-Forchheimer ferrofluid slip flow system. *Int. Commun. Heat Mass Transf.* **2021**, *129*, 105730. [CrossRef]

35. Soomro, F.A.; Alamir, M.A.; El-Sapa, S.; Haq, R.U.; Soomro, M.A. Artificial neural network modeling of MHD slip-flow over a permeable stretching surface. *Arch. Appl. Mech.* **2022**, *92*, 2179–2189. [CrossRef]

36. Shoaib, M.; Zubair, G.; Nisar, K.S.; Raja, M.A.Z.; Khan, M.I.; Gowda, R.P.; Prasannakumara, B.C. Ohmic heating effects and entropy generation for nanofluidic system of Ree-Eyring fluid: Intelligent computing paradigm. *Int. Commun. Heat Mass Transf.* **2021**, *129*, 105683. [CrossRef]
37. Raja, M.A.Z.; Shoaib, M.; Zubair, G.; Khan, M.I.; Gowda, R.P.; Prasannakumara, B.C.; Guedri, K. Intelligent neuro-computing for entropy generated Darcy-Forchheimer mixed convective fluid flow. *Math. Comput. Simul.* **2022**, *201*, 193–214. [CrossRef]
38. He, X.; Sidi, M.O.; Ahammad, N.A.; Elkotb, M.A.; Elattar, S.; Algelany, A.M. Artificial neural network joined with lattice boltzmann method to study the effects of mhd on the slip velocity of fmwnt/water nanofluid flow inside a microchannel. *Eng. Anal. Bound. Elem.* **2022**, *143*, 95–108. [CrossRef]
39. Safaei, M.R.; Hajizadeh, A.; Afrand, M.; Qi, C.; Yarmand, H.; Zulkifli, N.W.B.M. Evaluating the effect of temperature and concentration on the thermal conductivity of ZnO-TiO2/EG hybrid nanofluid using artificial neural network and curve fitting on experimental data. *Phys. A Stat. Mech. Its Appl.* **2019**, *519*, 209–216. [CrossRef]
40. Khan, M.I.; Shoaib, M.; Zubair, G.; Kumar, R.N.; Prasannakumara, B.C.; Mousa, A.A.A.; Malik, M.Y.; Raja, M.A.Z. Neural artificial networking for nonlinear Darcy–Forchheimer nanofluidic slip flow. *Appl. Nanosci.* **2022**, 1–20. [CrossRef]
41. Çolak, A.B.; Shafiq, A.; Sindhu, T.N. Modeling of Darcy–Forchheimer bioconvective Powell Eyring nanofluid with artificial neural network. *Chin. J. Phys.* **2022**, *77*, 2435–2453. [CrossRef]
42. Bala Anki Reddy, P.; Jakeer, S.; Thameem Basha, H.; Reddisekhar Reddy, S.R.; Mahesh Kumar, T. Multi-layer artificial neural network modeling of entropy generation on MHD stagnation point flow of Cross-nanofluid. *Waves Random Complex Media* **2022**, 1–28. [CrossRef]
43. Toghraie, D.; Sina, N.; Jolfaei, N.A.; Hajian, M.; Afrand, M. Designing an Artificial Neural Network (ANN) to predict the viscosity of Silver/Ethylene glycol nanofluid at different temperatures and volume fraction of nanoparticles. *Phys. A Stat. Mech. Its Appl.* **2019**, *534*, 122142. [CrossRef]
44. Dey, P.; Sarkar, A.; Das, A.K. Prediction of unsteady mixed convection over circular cylinder in the presence of nanofluid-A comparative study of ANN and GEP. *J. Nav. Archit. Mar. Eng.* **2015**, *12*, 57–71. [CrossRef]
45. Qureshi, I.H.; Awais, M.; Awan, S.E.; Abrar, M.N.; Raja, M.A.Z.; Alharbi, S.O.; Khan, I. Influence of radially magnetic field properties in a peristaltic flow with internal heat generation: Numerical treatment. *Case Stud. Therm. Eng.* **2021**, *26*, 101019. [CrossRef]